TESTS OF A PROTECTIVE SHELL PASSIVE RELEASE MECHANISM FOR HYPERSONIC WIND-TUNNEL MODELS

Richard L. Puster* and James E. Dunn**

ABSTRACT

A protective shell mechanism for wind tunnel models was developed and tested. The mechanism is passive in operation, reliable, and imposes no new structural design changes for wind tunnel models. Methods of predicting the release time and the measured loads associated with the release of the shell are given. The mechanism was tested in a series of wind tunnel tests to validate the removal process and measure the pressure loads on the model. The protective shell can be used for wind tunnel models that require a step input of heating and loading such as a thin skin heat transfer model. The mechanism may have other potential applications.

INTRODUCTION

Hypersonic wind tunnel models sometimes require protection from pressure loads associated with the start or unstart of the wind tunnel, the loads caused by insertion into the test stream, and thermal and aerodynamic loads of the test medium until exposure of the model is desired. A passive system has been developed which shields a wind tunnel model from a hot hypersonic test medium and then exposes the model to a step input of aerodynamic heating and loading - a useful technique for experimental heat transfer studies. The protection system is novel in that no active electrical, mechanical, or explosive devices are required for the removal of the protective shell.

This paper will describe the design and performance of a protective shell mechanism that was tested in a wind tunnel to verify the operation of the mechanism and to measure the transient loads associated with the release of the protective shell.

SYMBOLS

h	heat transfer coefficient (W/m^2-K)
I	impulse (N/s)
K	heat input parameter (equation 1)
L	model length (cm)
M	Mach number
N_R	Unit Reynolds number per m
P	pressure (kPa or MPa)
$\overline{P}$	mean pressure (kPa or MPa)

*NASA Langley Research Center, Hampton, VA
**Prototype Development Associates, Santa Ana, CA

r	radius (cm)
R	gas constant $\frac{J}{kmol-K}$
s	surface distance (see figure 5)
t	time (s)
T	temperature (K)
$\overline{T}$	mean temperature (K)
X	axial distance along model (cm)
σ	standard deviation

Subscript:

b	base
c	cone
CI	center of impulse
oc	plenum conditions in combustor
p	test section pod
o	total or stagnation point or first exposure of forward split nut to aerodynamic heating
w	wall
zr	temperature at retaining ring failure
1	time to retaining ring failure
2	pitot or time for cavity between model and shell to fill and aft retaining ring to break
3	total time required for all of protective shell components to be downstream of model
∞	freestream

TEST MODEL ASSEMBLY AND OPERATION

Protective Shell Assembly

Figure 1 illustrates the components of the protective shell and the wind tunnel model. The shell was made of two longitudinally split fiberglass petals formed with support pads as shown in the figure. The petals are held in place by a forward restraint/release nut and an aft restraint band. The forward split release nut, shown in detail in figure 2, was fabricated of low brass (80% Cu;

20% Zn) in two pieces which were held together by a zinc retaining ring. The brass nut halves were lap finished at the part plane to produce essentially zero clearance when assembled. A zinc retaining ring was fitted into a circular groove at the rear of the nut, compressed to twice the yield strength of the zinc, and the excess zinc was then machined flush with the brass. A hole was then drilled and tapped into the aft face of the assembled nut. A brass bolt with a conical head was made to nest inside a matching internal conical cavity in the split halves of the petal. By screwing the split nut onto the bolt, the protective petal halves were held and compressed together at the forward end. At the aft end of the model an adaptor ring was installed on the base of the cone and the petal halves were held in place by an external, frangible fiberglass band.

Model

The wind tunnel model was a spherically blunted, 15 degree half-angle cone with a 3.6 cm nose radius, a length of 61 cm, and a base diameter of 38 cm. The model had a gas driven impulse turbine permitting it to be rotated between 1 to 5 revolutions per second. A photograph of the assembled model in the test section of the wind tunnel is shown in figure 3. A device was installed at the base of the model to catch the adapter ring for reuse and to prevent damage to the adapter ring or the model support sting.

The purpose of the rotation was to make the investigation general in scope so that the results could be applied to freely spinning flight bodies. Most wind tunnel models do not rotate and are inserted into the test medium at a zero degree angle of attack; therefore the release dynamics were investigated at this condition as well.

Operational Mechanism

The protective shell removal mechanism is relatively simple. When the model is inserted into the flow, aerodynamic heating to the split nut transfers heat inward raising the temperature of the retaining ring. When the retaining ring is hot enough to lose its strength the two halves of the split nut separate, exposing the annulus between the model and its protective shell to high aerodynamic pressure. As the petal-model annulus fills, the petals open further and break the aft restraining band. As a result of aerodynamic forces, the bolt and petals move away and outward from the model. Freestream turbulence, gravity, and flow misalignment cause the bolt to be removed from the nose. The petals fracture, and the fragments, the bolt, split nut halves, and the parts of the aft restraint band are all accelerated downstream.

Instrumentation

The model had twenty semiconductor pressure transducers (see ref. 1 and 2 for a description of this type of transducer). The temperature of the retaining ring of the forward split nut was measured using two spring loaded chromel alumel thermocouples mounted through the bolt. The spin rate of the model was measured using a fixed Hall effect proximity sensor and permanent magnets rotating with the model. A blunt nose with the same geometry as the forward split nut was made and instrumented with four Gardon-type heat flux gages and was used in separate tests to measure heat flux and its distribution on the flat faced portion of the nose. In another series of tests a sharp cone was fitted to the model and used with the surface pressure transducers to calibrate the test flowfield. Motion picture coverage at 400 and 1000 fps was used to record the protective shield removal process.

FACILITY AND TEST CONDITIONS

The tests were performed in the Langley 8-Foot High-Temperature Structures Tunnel, a hypersonic blow down wind tunnel. The high-energy test stream consists of the products of combustion obtained from a mixture of methane and air burned under pressure in a plenum chamber. The flow is expanded through an axisymmetric, contoured nozzle to approximately Mach 7 into an open-jet test section. The flow is decelerated in a supersonic diffuser. Additional information about the facility and test procedures may be found in references 3, 4, and 5. The nominal test conditions are given in Table I. The stream gas composition, the thermodynamic, transport and flow properties, used for calculating heat flux and flow parameters, were calculated from a thermochemical computer code (ACE) described in reference 6. There was no particular flight condition simulated although the equivalent earth altitude is listed in Table I for reference. The matrix of test conditions provided a range of variables including heat flux, spin rate, angle of attack, model pressure, and freestream pressure.

DATA ACQUISITION AND SPECIAL COMPUTATIONAL TECHNIQUES

Data Acquisition

The information from model test sensors consists of low frequency data such as the temperature rise of the retaining ring, and very high frequency data, such as the transient surface pressures during the petal removal process. The output of the gages was recorded at 20 samples per second on a low frequency system filtered at 2 Hz, and concurrently on two FM tape recorders. The signal from the gages was input to each system with an isolation amplifier with a gain of 1. The FM recorded signal was flat to within 1 db up to 20 kHz. The FM data were sampled at 50×10^3 samples per second to prevent aliasing (see ref 7) and filtered at 12.5 kHz using a sharp rolloff constant amplitude filter (48 db/octave). Consequently the data should be accurate to at least 10 kHz. Ground loop electrical noise at 60 Hz was present but was of such a low magnitude that the transient data were unaffected and because of the 2 Hz filter the low frequency data were not affected at all.

Flowfield Calibration

The flowfield and the conditions at the surface of the cone in particular were calculated with the use of the gas properties calculated from reference 6 and used as input to the program of reference 8. Figure 4 presents the results of some of those calculations. The ratio of cone surface pressure to free-stream static pressure is given as a function of freestream Mach number for air and various total temperatures of the combustion products. The information from reference 9 was used to verify the computational method of reference 8 for air. It is evident from figure 4 that as the total temperature increases there is a significant difference between the values of the cone to freestream pressure ratio for air and for combustion products over the Mach number range shown.

The tunnel conditions were assumed to be constant for the capture diameter (38 cm.) of the cone. This is a reasonable assumption since the flowfield diameter is 244 cm and previous calibrations, reference 10, have indicated that the flowfield is fairly uniform over a 102 cm diameter of the center of the wind tunnel. Using the sharp nose cone with the bare wind tunnel model and by varying the position of the support strut, the flow Mach number and its radial distribution were determined with the use of the curves of figure 4. The flow

for the test conditions of Table I has a mean Mach number of 6.75 with a standard deviation about the mean of 0.077 (σ) for the central 2 m core of the flow.

PREDICTION TECHNIQUES

In order to predict when the release of the forward split nut would occur, it was necessary to utilize a good heat transfer prediction; measure the actual heat flux; develop a release time prediction; and correlate the parameters. The following sections will elaborate on each topic.

Heat Transfer Prediction and Measurement

The heat transfer coefficient distribution about the face and after body of the forward split nut was calculated using the methods of references 11 and 12 and the gas properties calculated by reference 6. Tests were made using the blunt nose with the Gardon type heat flux gages and yielded the heat transfer coefficient distribution shown in figure 5 to an s/r_b of 0.65. The results shown are for an angle of attack of zero; all other conditions of angle of attack, spin rate, total pressure and temperature were measured but are not reported here. The heat transfer coefficient distribution was calculated and measured in reference 11 for air at a Mach number of 8.0. The agreement between the coefficient distribution for air and that of the present test as shown in figure 5, using combustion products was very good. The continuous increase in heat transfer coefficient can be substantiated by similar distributions found in references 13 and 14. In all these references and in the present tests, the unit Reynolds number of the flow was high (at least 3 million per m) and the flow hypersonic. Since the flat face geometry of both was identical (up to $s/r_b = 0.81$) and the Mach number and Reynolds number were similar, the coefficient distribution up to an s/r_b of 0.81 from reference 11 was plotted and used in figure 5. The distribution about the rest of the forward split nut was calculated using the methods of reference 12 and a modified Newtonian pressure distribution. Other methods of predicting heat transfer are reviewed in reference 15; in general the methods yield values that can vary up to 10 percent from each other. The agreement between the measured values and the curve from reference 11 gives good confidence for the technique used.

Split Nut Release Time Prediction

Using the computer code SINDA of reference 16 and the combined measured and calculated heat input distribution, the temperature of the surface and inner temperatures of the brass split nut and zinc retaining ring were calculated as functions of time and position. A typical result of these calculations is shown in figure 6. Figure 6 shows the calculated internal temperature distribution of the forward split nut and zinc retaining ring at the zinc retaining ring failure time. Based on the results of the calculations, the zinc should melt in about 20 seconds for the conditions shown and the split nut should then come apart.

Release Time-Heat Load Correlation

A simplified method of predicting stagnation heat flux was developed in reference 17. Eckert's reference temperature was used and a Lewis number of one (no dissociation) was assumed. The derived expression was compared

with that of Fay and Riddell (reference 18) and found to agree within about one percent. By using the methods of reference 17, the maximum variation of the measured stagnation heat transfer coefficient from that calculated was about six percent.

A heat input parameter for use in release time correlation may be derived from the expressions of reference 17 for stagnation point heat transfer coefficient. Any variables found to have less than a 2 percent effect on the heat transfer coefficient were dropped to simplify the expression derived. The heat input was normalized such that the resulting parameter was less than 1.0 for this experiment. The resulting parameter, K, is given by:

$$K = \frac{\sqrt{P_{o,2}}\, T_o^{0.18}(T_o - \bar{T}_w)}{50{,}000} \tag{1}$$

where

$$\bar{T}_w = \frac{\int_{t_o}^{t_1} T_w \, dt}{t_1 - t_o} \tag{2}$$

The heat input parameter, K, will be used to correlate the release time of the split nut as a function of time.

RESULTS

Split Nut Release Time

In figure 7, the observed and calculated split nut release times, t_1, are plotted as a function of the parameter K. The calculated release time as shown in the figure agrees reasonably well with the experimental data with the agreement between theory and experiment being better for the longer duration tests (lower heat flux). Near the solidus point of the zinc alloy (645K for AG40A) used, the variations in strength and fabrication translate into variations in the release time of the split nut. The observed split nut release times and the failure temperature, T_{zr}, of the zinc retaining ring are tabulated in Table II. The observed temperature of the retaining ring at failure varied from 617 to 625K with a mean value of 622K. If the mean strength of the zinc was used as the most probable failure stress, then the retaining ring would fail at 625K which was the measured maximum failure temperature. Thus, the prediction techniques used appear to be valid and reasonably accurate.

Protective Shell Removal

The removal process can best be studied by observing the sequence of photographs of figure 8. As seen in the figure, after about 16 to 18 ms, the petals have opened enough so that the load on the aft restraint band causes it to fail. The petals move outward from the model and fracture, the split nut halves, the bolt, the fractured petals, and the broken aft restraint band are all accelerated downstream. In figure 8, the bolt remains on the nose since it was held there by the thermocouple assembly, which was mounted through the bolt and used to measure the zinc retaining ring temperature. When the

thermocouple assembly was not used the bolt left the nose as expected. In all of the observed tests (using eight (8) 1000 fps and four (4) 400 fps cameras on each test) the removal process was essentially the same, requiring about 35 to 60 milliseconds (see Table II). No model impacts by the components of the protective mechanism were observed even at the highest angle of attack ($\alpha = 9°$) and lowest rotational speed. The aft restraining band always broke before the petals fractured. However, at the highest angle of attack ($\alpha = 9°$) an additional 1/4 spin revolution was required before the windward petal flew outward from the model. In addition, the bolt, when not restrained by the thermocouples, left the nose and traveled downstream. Thus the removal process appears to be reliable; however, downstream tunnel components must be rugged to withstand the bolt and nut impacts.

The mechanism is most suitable for open circuit (usually blow down type) wind tunnels but could be employed in closed circuit wind tunnels which use capture nets to screen debris before return to the compressors. If the model does not spin, the mechanism can only be used when the angle of attack is zero or near zero.

Transient Loads

Figure 9 presents a typical low frequency model surface pressure history and figure 10 a typical transient pressure history of the cone surface. As can be seen from figure 9 the seams between the petals are not perfect and allow the pressure between the shell and model to increase above the test section static pressure but substantially lower than the surface pressure on the outer surface of the shell. However, there was no detectable heating of the model surface. As the split nut opens, the interior pressure increases at a faster rate; then the protective shell is removed and the pressure on the model quickly reaches the cone surface pressure. The transient pressure history is shown in detail on figure 10. The figure shows the background line 60 Hz noise; the frequency was determined by auto-correlating the signal before and after the shell removal. The smaller oscillations are caused by broadband turbulent boundary layer noise. The process of the pressurization of the cavity between the shell petals and the model requires about 14 to 18 ms, being faster for the higher stagnation pressure. The interior pressure increases to 1.5 to 3 times the cone surface pressure with the pressure rise being greater toward the aft end of the cavity. When this process has been completed, the load on the aft restraining band causes it to break. Immediately thereafter, the petals move outward with a consequent sharp drop in cone surface pressure. There may be one relatively slow, major amplitude, oblique shock wave, indicated by the sharp spike in pressure, or there may be two or more pressure spikes (fig. 10b). These transient pressures may occasionally reach 70 to 80 percent of the pitot pressure, but the most probable value observed is 50 percent or less of the pitot pressure with the amplitude of the shock wave decreasing towards the forward end of the cone.

The pressure history from each of the 20 pressure gages was integrated with respect to time, then area, and the impulse imposed on the model was calculated from

$$I = \sum_{n=1}^{20} \left(A_n \int_{t_o}^{t_3 - t_1} P \, dt \right) \qquad (3)$$

where A_n are equal surface area segments.

The effective location of the impulse relative to the body was also calculated. These values plus the cavity fill and removal times are tabulated in Table II. The impulse imparted to this model during the petal removal was usually less than 13 N/s at low angles of attack (0 to 3 degrees); however, at larger angles of attack (6 to 9 degrees), the lateral impulse varied from 36 to 53 N/s. These loads are still extremely low and should present no problem to any wind tunnel model or most flight vehicles.

Potential Applications

In addition to wind tunnel use, the mechanism could be used for the protection of axisymmetric high velocity research vehicles from particle or water impact damage or for heat transfer research. Other applications could be a protective shell for a planetary research probe. The mechanism is reliable, passive, and should be functional indefinitely.

CONCLUDING REMARKS

A protective shell mechanism has been developed that will shield a wind tunnel model and then expose the model to the hypersonic flow field. The mechanism is completely passive in that aerodynamic heating of a brass forward split nut, held together by a zinc retaining ring, caused the ring to fail and thus exposed the petals of the protective sehll to aerodynamic loading. As the cavity pressure between the model and shell petals increases, the loading on an aft restraint band causes it to break. Then, all of the components of the protective shell mechanism are accelerated downstream and out the wind tunnel diffuser. The expected removal process was validated by a series of wind tunnel tests that included varying the heat input, the model angle of attack, and spin rate. The time required for the release process to begin could be calculated with reasonable accuracy and the removal process occurred in 60 ms or less. The mechanism worked reliably with no model strikes from shell components, although at the highest angle of attack an additional 1/4 revolution was required to separate the windward petal. Transient surface pressures were measured and the net lateral impulse delivered to the model was usually less than 15 N/s for angles of attack below 3 degrees; however at larger angles of attack (6 to 9 degrees) the impulse varied from 36 to 53 N/s. The protective shell mechanism can be used for wind tunnel models and has potential application to high velocity research vehicles.

REFERENCES

1. Kurtz, A. D.; and Gravel, C. L.: Semiconductor Transducers Using Tranverse and Shear Piezoeresistance. 22nd ISA Conference, Chicago, September, 1967.

2. Kurtz, A. D.; and Kicks, J. S.: Development and Applications of High Temperature Ultra-Miniature Pressure Transducers. ISA Silver Jubilee Conference, October 1970, Philadelphia.

3. Schaefer, William T., Jr.: Characteristics of Major Active Wind Tunnels at the Langley Research Center. NASA TMX-1130, 1965.

4. Howell, R. R.; and Hunt, L. R.: Methane - Air Combustion Gases as an Aerodynamic Test Medium. Journal of Spacecraft and Rockets, Vol. 9 No. 1 January 1972.

5. Hunt, L. Roane: Aerodynamic Heating and Loading Within Large Open Cavities in Cone and Cone-Cylinder-Flare Models at Mach 6.7. NASA TN D-7403.

6. Kendall, Robert M.: An Analysis of the Coupled Chemically Reacting Boundary Layer and Charring Ablator. Part V - A General Approach to the Thermochemical Solution of Mixed Equilibrium - Nonequilibrium, Homogeneous or Heterogeneous Systems. NASA CR-1064, 1968.

7. Bendat, Julius, S.; Piersol, Allan G.: Measurement and Analysis of Random Data. John Wiley, New York, 1966.

8. Prozan, R. J.: Solution of Non-Isoenergetic Supersonic Flows by Method of Characteristics. Volume III. NASA CR-132274, July 1971.

9. Sims, Joseph L.: Tables for Supersonic Flow Around Right Circular Cones at Zero Angle of Attack. NASA SP-3004, 1964.

10. Deveikis, William D.; and Hunt, L. Roane: Loading and Heating of a Large Flat Plate at Mach 7 in the Langley 8-Foot High-Temperature Structures Tunnel, NASA TN D-7275, 1973.

11. Jones, Robert A.: Heat Transfer and Pressure Distributions on a Flat-Face Rounded-Corner Body of Revolution With and Without a Flap at a Mach Number of 8. NASA TMX-703, September, 1962.

12. Beckwith, Ivan E.; and Cohen, Nathaniel: Application of Similar Solutions to Calculations of Laminar Heat Transfer on Bodies with Yaw and Large Pressure Gradient in High-Speed Flow. NASA TN D-625, 1961.

13. Cooper, Morton; and Mayo, Edward E.: Measurements of Local Heat Transfer and Pressure on Six 2-Inch Diameter Blunt Bodies at A Mach Number of 4.95 and At Reynolds Numbers Per Foot Up to 81 x 10^6. NACA Memo 1-3-59L, March, 1959.

14. Stalmach, C. J., Jr.; and Goodrich, W. D.: Aeroheating Model Advancements Featuring Electroless Metallic Plating. AIAA 9th Aerodynamic Testing Conference. Arlington, Texas, June 7-9, 1976.

15. Hoshizaki, H.; Chou, Y. S.; Kulgein, N. G.; and Meyer, J. W.: Critical Review of Stagnation Point Heat Transfer Theory. AFFDL-TR-75-85, July, 1975.

16. Gaski, J. D.; Fink, L. C.; and Ishimoto, T.: Systems Improved Numerical Differencing Analyzer. NASA Contract 9-8289 and 9-10435 Sept. 1970 and April 1971, TRW Systems Inc., Redondo Beach, California.

17. Buckley, Frank T.: Constant-Mach-Number Simulation of Critical Flight Loads on High-Velocity Projectile Fuses. Harry Diamond Lab TR-1466, August 1969.

18. Fay, J. A. and Riddell, F. R.: "Theory of Stagnation Point Heat Transfer in Dissociated Air," JAS, V.25, 73 (1959).

TABLE I. TEST CONDITIONS

TEST	$\bar{P}_{oc}$*	$P_{0,2}$	$\bar{T}_{oc}$		FREE-STREAM DYNAMIC PRESSURE	P_∞	ANGLE OF ATTACK	N_R	ROTATIONAL SPEED OF MODEL	EQUIVALENT EARTH ALTITUDE
	MPa	kPa	K	$\sigma/\bar{T}_{oc}$	kPa	kPa	deg	per m $\times 10^6$	rev per s	km
1	18.27	136.1	1860	0.030	72.0	2.83	0	4.62	1.4†	24.3
2	18.38	136.9	1860	0.030	74.2	2.52	0	5.00	3.6	25.1
3	18.25	136.0	1858	0.025	73.6	2.50	3	4.93	2.0	25.1
4	18.31	137.3	1823	0.033	73.4	2.50	6	4.80	2.5	25.1
5	10.86	74.40	1561	0.030	38.0	1.49	0	3.02	4.4	28.5
6	10.86	81.43	1831	0.036	43.3	1.47	0	2.67	4.2	28.6
7	10.85	80.33	1741	0.037	42.0	1.50	6	2.81	3.3	28.5
8	10.85	80.06	1729	0.030	41.4	1.49	9	2.88	2.6	28.5

* - $\sigma/\bar{P}_{oc}$ WAS USUALLY 0.0025 OR LESS

† - REPEATED AT ZERO ROTATIONAL SPEED

TABLE II. SUMMARY OF TEST RESULTS

TEST	t_1-t_0	t_2-t_1	t_3-t_1	T_{zr}	I	$X_{CI/L}$
	s	ms	ms	K	N/S	
1	19.55	17	55	617	12.9	0.30
2	20.80	16	55	622	11.6	0.99
3	20.05	17	45	622	14.2	0.47
4	20.69	15	60	622	51.2	0.68
5	33.18	17	60	625	9.8	0.94
6	27.67	23	45	*	11.1	0.75
7	27.41	25	65	622	42.7	0.75
8	28.62	23	35 205†	*	35.6	0.74

* - RETAINING RING THERMOCOUPLES NOT USED SO BOLT BEHAVIOR COULD BE EVALUATED

† - TIME OF SECOND PETAL REMOVAL

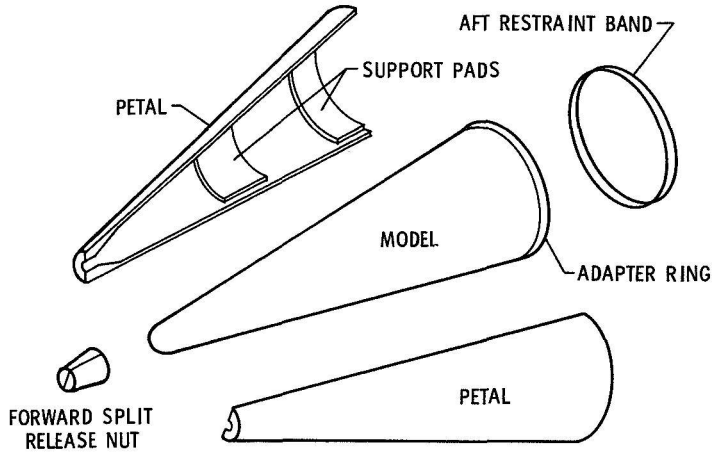

Figure 1.- Protective shell mechanism components.

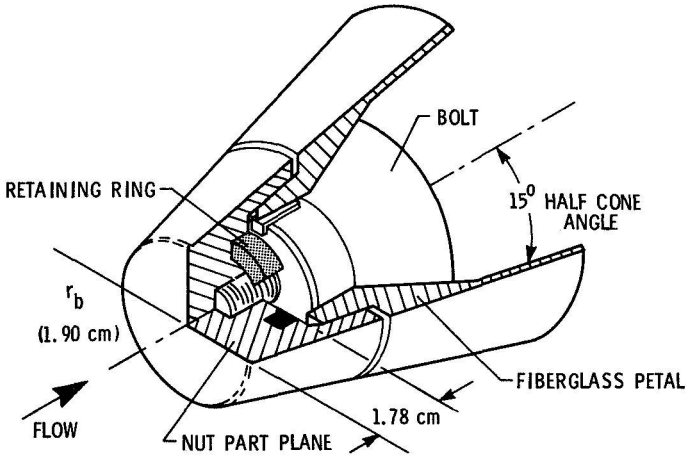

Figure 2.- Details of split release nut.

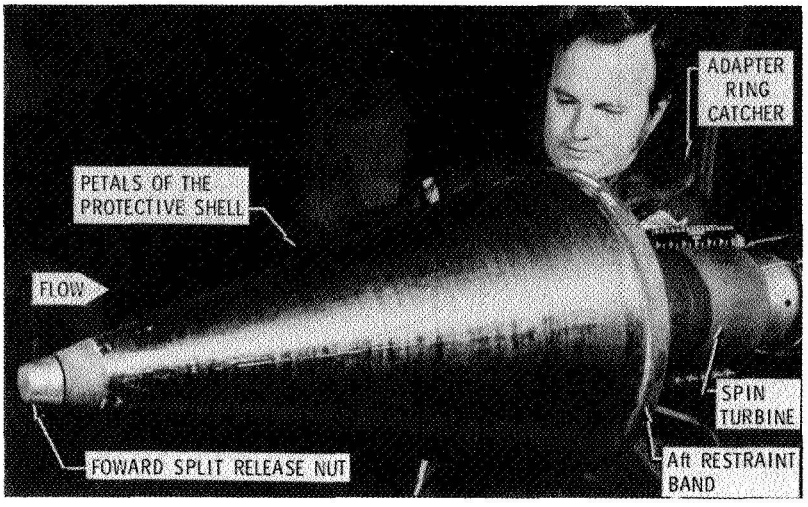

Figure 3.- Assembled model in test section of wind tunnel.

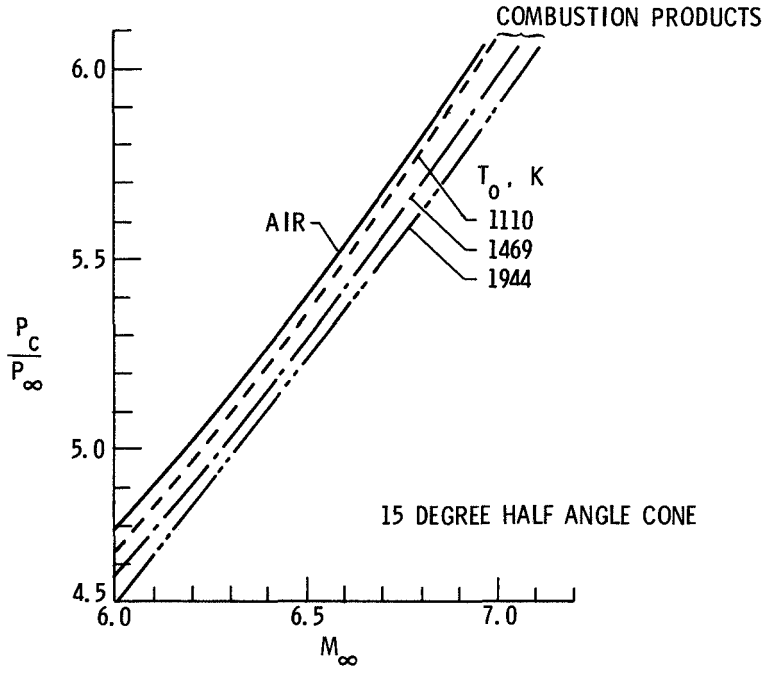

Figure 4.- Variation of cone to freestream pressure ratio with freestream Mach number

	h_o, W/m^2 - K	M_∞	$N_R \times 10^6$	T_o, K	P_o, MPa	TEST GAS
O	509	6.75	4.92	1808	18.2	COMBUSTION PRODUCTS
—	210	8.0	3.05	728	6.31	AIR (REF. 11)
---	CALCULATED FOR THIS TEST FOR $s/r_b > 0.81$					

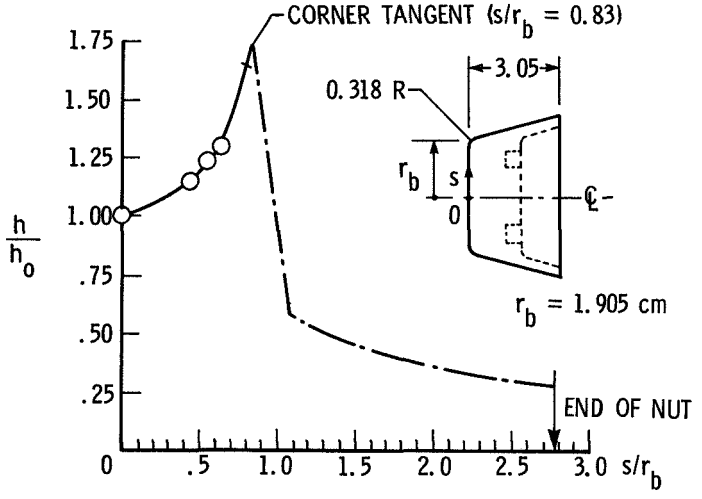

Figure 5.- Variation of heat transfer coefficient over surface of forward split release nut.

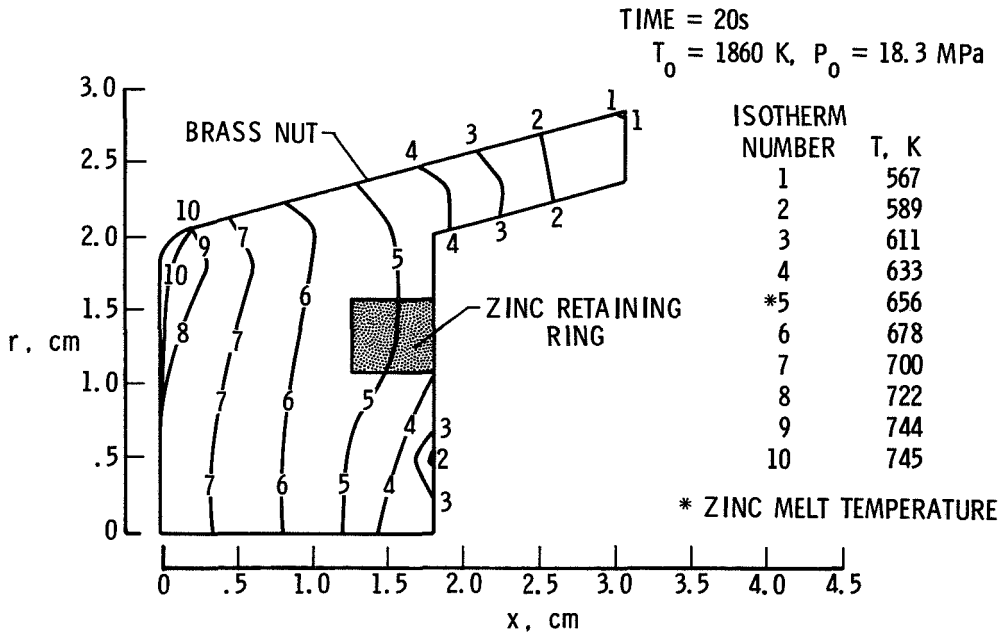

Figure 6.- Contour plot of isotherms through the nut and zinc retaining ring.

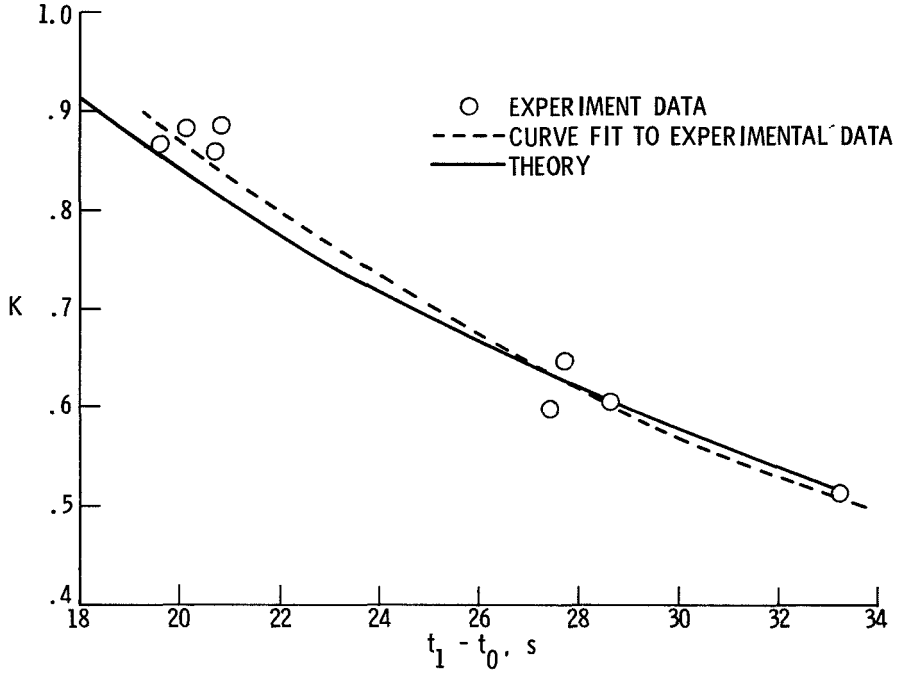

Figure 7.- Comparison of the calculated and experimental split nut release times.

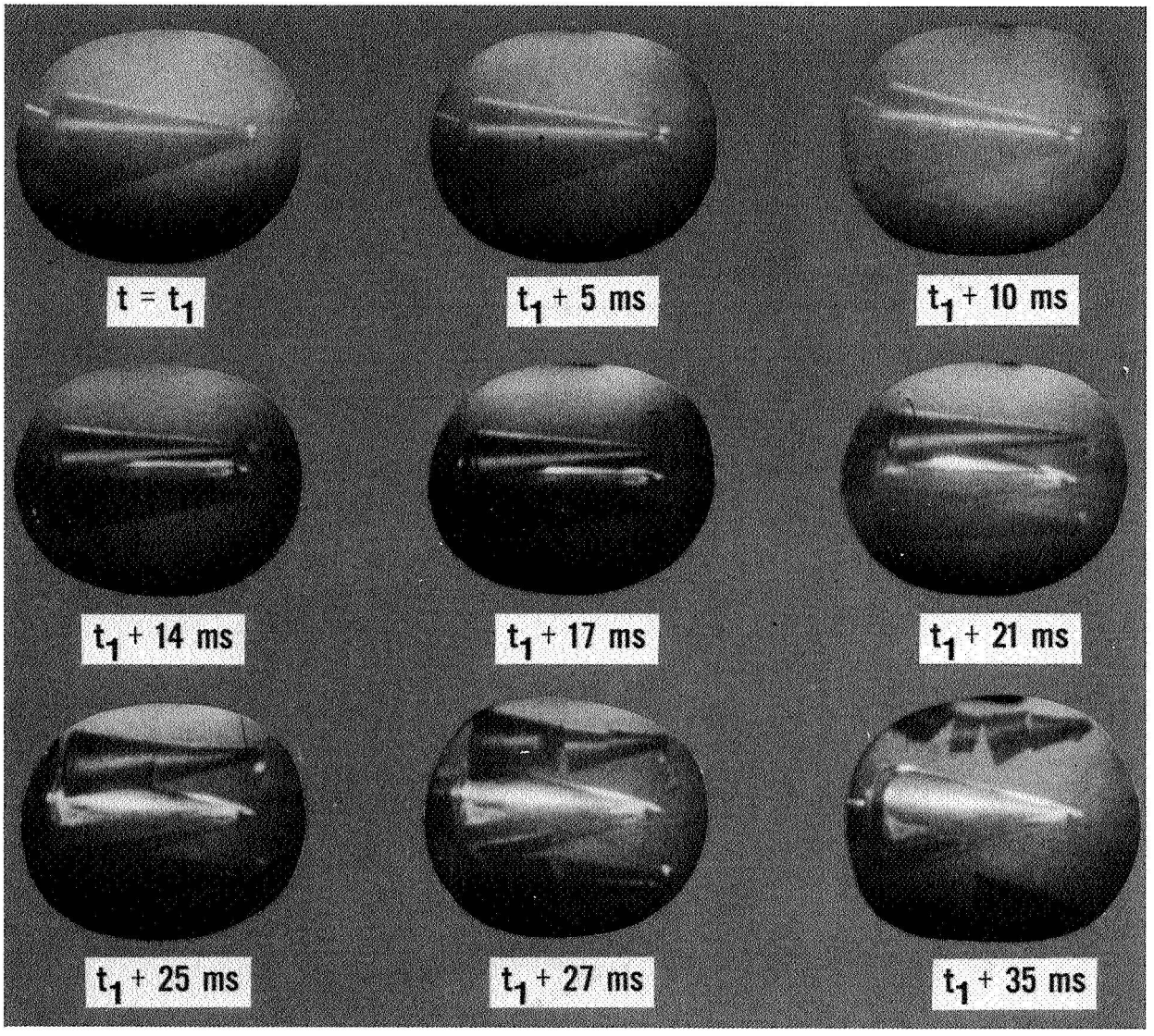

Figure 8.- Removal sequence of protective shell.

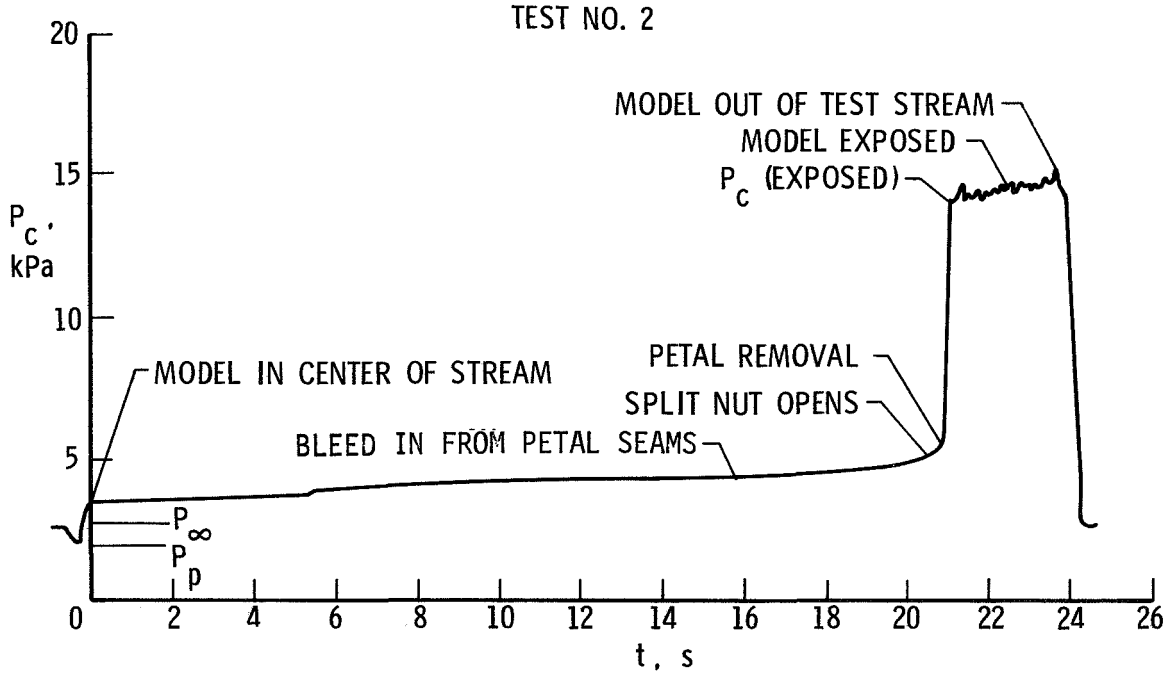

Figure 9.- Cone surface pressure during a typical test.

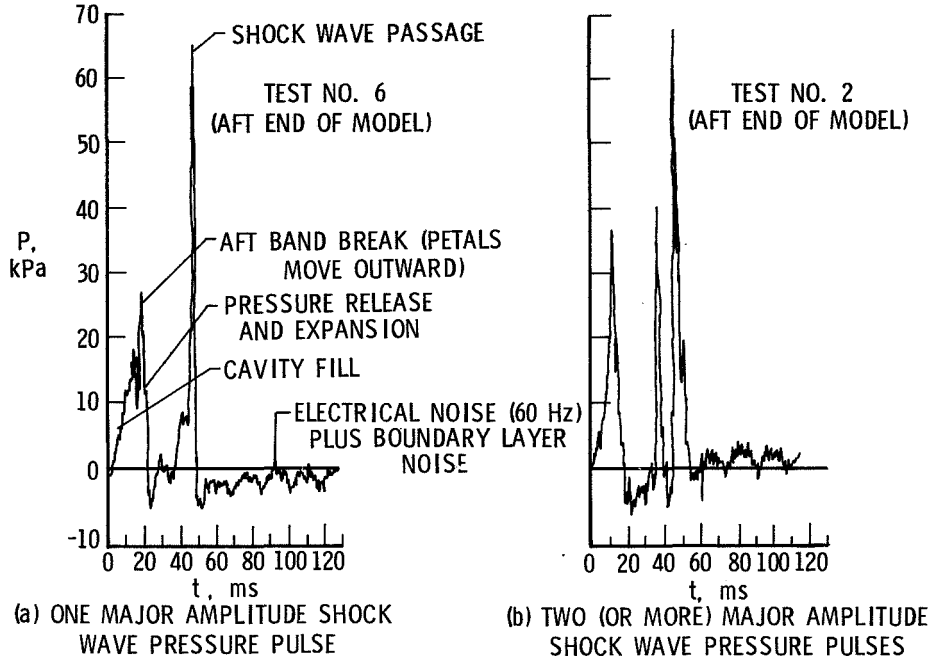

Figure 10.- Dynamic pressure history of cone surface during petal removal.